We are IntechOpen, the world's leading publisher of Open Access books
Built by scientists, for scientists

4,800
Open access books available

122,000
International authors and editors

135M
Downloads

Our authors are among the

154
Countries delivered to

TOP 1%
most cited scientists

12.2%
Contributors from top 500 universities

CLARIVATE ANALYTICS
BOOK CITATION INDEX
INDEXED

WEB OF SCIENCE™

Selection of our books indexed in the Book Citation Index in Web of Science™ Core Collection (BKCI)

Interested in publishing with us?
Contact book.department@intechopen.com

Numbers displayed above are based on latest data collected.
For more information visit www.intechopen.com

Chapter

Knock Suppression of a Spark-Ignition Aviation Piston Engine Fuelled with Kerosene

Enhua Wang, Chenyao Wang, Fujun Zhang, Huasheng Cui, Chuncun Yu, Bolan Liu, Zhenfeng Zhao and Changlu Zhao

Abstract

Spark-ignition (SI) engine has a high power density, making it suitable for unmanned aerial vehicles. Normally, gasoline fuel with a high octane number (ON) is used for a spark-ignition engine. However, gasoline fuel is easy to be evaporated and has a low flash point which is unsafe for aviation engines. Kerosene with a high flash point is safer than gasoline. In this chapter, the combustion characteristics of kerosene for a spark-ignition aviation piston engine are analyzed. A three-dimensional (3D) model is setup, and the combustion process of the engine fuelled with kerosene is simulated. Later, the knock limit extension by water injection is evaluated experimentally. The results indicate that water injection can suppress the knock of SI engine with kerosene in some extent and the output power can be improved significantly.

Keywords: aviation piston engine, spark ignition, kerosene, knock suppression, water injection

1. Introduction

Four-stroke spark-ignition (SI) piston engines have advantages of good fuel economy, high power to weight density, low noise, low cost, and easy maintenance, making them suitable for helicopters and unmanned aerial vehicles [1]. However, gasoline is volatile and easy to be ignited, which is not safe as aviation fuel. In contrast, kerosene is safer and has been used widely for airplanes. If gasoline can be replaced by kerosene on a four-stroke SI piston engine, the aviation safety will be improved significantly. Therefore, the combustion characteristics of four-stroke SI piston engine using kerosene as fuel need to be investigated.

The physical properties of kerosene are very different from gasoline. Kerosene has a lower volatility and higher viscosity. Accordingly, the spray penetration, spray velocity, and cone angle are different [2]. As a wide distillation fuel, the chemical properties of kerosene also differ from gasoline. Lots of experiments were conducted to investigate the combustion characteristics of kerosene [3, 4]. For example, the ignition delay time of kerosene was measured as a function of temperature, pressure, and equivalence ratio using a shock tube [5] or laser-induced fluorescence (LIF) imaging [6].

The combustion performance of kerosene has been investigated comprehensively for turbojet and scramjet engines [7, 8]. However, the operation conditions of

aviation piston engine deviate from those of turbojets and scramjets significantly. Very few investigations focused on the combustion performance of kerosene for internal combustion engines [9–11]. Fernandes et al. studied the performance of a heavy-duty diesel engine fuelled with JP-8. The torque output and fuel consumption were similar with diesel fuel. However, the injection duration was enlarged to compensate the low fuel density, and the ignition delay time was increased because of a low cetane number. In addition, the emissions of nitrogen oxide (NOx) and particle material (PM) were decreased apparently [12]. Tay et al. developed a reaction mechanism composed of 48 species and 152 reactions for kerosene, and the accuracy was validated in an optical engine [13].

Generally, the octane number (ON) of gasoline is in the range of 70–97, whereas the octane number of kerosene is much lower as only 20–50. Therefore, the knock phenomenon of kerosene is much severe in an SI engine, which will keep the power and economy of the engine in a low level [14]. To control the knock of an SI engine, various methods can be adopted, for example, postponing ignition time, reducing compression ratio, and using antiknock additives. Recently, water injection got wide attentions to control the super knock of gasoline engine [15]. There are basically two methods: port water injection and in-cylinder direct water injection. When port water injection is employed, water is sprayed into the intake manifold. For direct water injection, water is injected directly into the combustion chamber. For port water injection, it is better to install the injector close to the intake valve. The knock suppression was increased for a mass ratio of water over fuel as 0.3 [16]. An experimental study based on a single-cylinder engine indicated that fuel with a lower octane number could be used if port water injection was installed [17]. Kim et al. performed an experiment, and water was sprayed into the cylinder in a pressure of 5 MPa using a gasoline direct injection (GDI) fuel injector. The knock suppression was observed evidently [18]. Wei et al. investigated the influences of water injection quantity on energy efficiency experimentally, and it was found that the energy efficiency maximized with a mass ratio of 0.15 [19].

For the knock suppression of SI aviation piston engine, Anderson et al. had studied the combustion performance of a Rotax 914 engine fuelled with kerosene blends. The octane numbers of the fuel blends were 87 and 70 via blending 100 ON aviation gasoline and JP-8. The brake mean effective pressure reduced evidently when the octane number of the fuel blends diminished. The effect of adjusting the ignition timing was very small for performance improvement [20]. Subsequently, the influences of mass fraction of JP-8 were investigated. The volume ratio of JP-8 changed from 85–27% blending with an 87 ON fuel. To keep a high engine power output, the volume ratio should be decreased accordingly [21]. Later, they used a pre-chamber jet ignition system to increase the flame propagation speed of kerosene, and the fuel octane number was decreased by about 10 [22].

It is critical to find methods that can suppress the knock for an aviation four-stroke SI engine with kerosene. However, very few investigations were performed currently. In this chapter, the knock suppression of an aviation four-stroke SI engine is investigated numerically at first. Then, port water injection is installed, and the experimental results for knock suppression are measured. The improvement of the indicated mean effective pressure (IMEP) is evaluated.

2. Mathematical method

The combustion of SI piston engine is mainly a turbulent flame propagation process. For the flow process in the cylinder, the mass, momentum, energy, and species conservation equations are modeled in the 3D numerical simulation model.

Mass:

$$\frac{\partial \rho}{\partial t} + \frac{\partial}{\partial x_i}(\rho u_i) = 0. \tag{1}$$

Momentum:

$$\frac{\partial}{\partial t}(\rho u_i) + \frac{\partial}{\partial x_i}\left(\rho u_i u_j\right) = -\frac{\partial p}{\partial x_i} + \mu \frac{\partial}{\partial x_i}\left(\frac{\partial u_i}{\partial x_j} + \frac{\partial u_j}{\partial x_i} - \frac{2}{3}\delta_{ij}\frac{\partial u_k}{\partial x_k}\right). \tag{2}$$

Energy:

$$\frac{\partial}{\partial t}(\rho h) + \frac{\partial}{\partial x_j}\left(\rho u_j h\right) = \frac{\partial p}{\partial t} + \frac{\partial}{\partial x_i}\left[\frac{\mu}{Pr}\frac{\partial h}{\partial x_j} + \frac{\mu}{Pr}\left(\frac{Pr}{Sc} - 1\right)\sum_{s=1}^{N} h_s \frac{\partial Y_s}{\partial x_j}\right]. \tag{3}$$

Species:

$$\frac{\partial}{\partial t}(\rho Y_s) + \frac{\partial}{\partial x_j}\left(\rho u_j Y_s\right) = \frac{\partial}{\partial x_j}\left(\frac{\mu}{Sc}\frac{\partial Y_s}{\partial x_j}\right) + \rho \dot{r}_s. \tag{4}$$

The density of the fluid is calculated by the following equation according to the equation of state for gaseous mixture.

$$\rho = p/\left[RT\sum_{s=1}^{N}(Y_s/M_s)\right]. \tag{5}$$

The enthalpy of the mixture can be calculated as

$$h = \sum_{s=1}^{N} Y_s h_s(T). \tag{6}$$

The above equations can be used in direct numerical simulation of turbulence, but it is difficult for the actual calculation process because the calculation load is extremely large. In this study, k - ε model is employed to simulate the turbulent flow in the cylinder. The turbulent eddy viscosity is defined as

$$\mu_t = C_\mu \overline{\rho} k^2/\varepsilon. \tag{7}$$

The transport equations for the turbulent kinetic energy k and the dissipation rate ε are expressed by

$$\overline{\rho}\tilde{u}_j \frac{\partial k}{\partial x_j} = \frac{\partial}{\partial x_j}\left[\left(\frac{\mu_t}{\sigma_k} + \mu\right)\frac{\partial k}{\partial x_j}\right] - \overline{\rho}\widetilde{u_i'' u_j''}\frac{\partial \tilde{u}_i}{\partial x_j} - \frac{\mu_t}{\overline{\rho}^2}\frac{\partial \overline{\rho}}{\partial x_i}\frac{\partial \overline{p}}{\partial x_i} - \overline{\rho}\varepsilon, \tag{8}$$

$$\overline{\rho}\tilde{u}_j \frac{\partial \varepsilon}{\partial x_j} = \frac{\partial}{\partial x_j}\left[\left(\frac{\mu_t}{\sigma_\varepsilon} + \mu\right)\frac{\partial \varepsilon}{\partial x_j}\right] - C_1\frac{\varepsilon}{k}\left[\overline{\rho}\widetilde{u_i'' u_j''}\frac{\partial \tilde{u}_i}{\partial x_j} + \frac{\mu_t}{\overline{\rho}^2}\frac{\partial \overline{\rho}}{\partial x_i}\frac{\partial \overline{p}}{\partial x_i}\right] - C_2\overline{\rho}\frac{\varepsilon^2}{k}. \tag{9}$$

The empirical constants for the standard k-ε model are assigned below: C_1 = 1.44, C_2 = 1.92, C_μ = 0.09, σ_k = 1.0, and σ_ε = 1.3. A nonslip boundary condition is assumed regarding all solid surfaces of the computational domain, and the standard wall functions are used.

The chemical time scales are assumed being much smaller than the turbulent ones. Therefore, the coherent flame model is used for the turbulent premixed combustion of the kerosene. The mean turbulent reaction rate is defined as

$$\overline{\rho \dot{r}_{fu}} = -\rho_{fr} y_{fu,fr} S_L \Sigma, \tag{10}$$

where S_L is the mean laminar burning velocity and Σ is the flame surface density. The transport equation for the flame surface density is

$$\frac{\partial \Sigma}{\partial t} + \frac{\partial}{\partial x_j}\left(\overline{u}_j \Sigma\right) - \frac{\partial}{\partial x_j}\left(\frac{v_t}{\sigma_\Sigma}\frac{\Sigma}{\partial x_j}\right) = S_g - S_a + S_{LAM}, \tag{11}$$

where σ_Σ is the turbulent Schmidt number, v_t is the turbulent kinematic viscosity, S_g is the product of the turbulent strain rate and the flame surface, S_a is the annihilation of flame surface, and S_{LAM} is the contribution of laminar combustion.

The laminar flame speed can be computed as

$$S_L = S_{L0}\left(1 - 2.1 y_{EGR}\right)\left(\frac{T_{fr}}{T_{ref}}\right)^{a_1}\left(\frac{p}{p_{ref}}\right)^{a_2}, \tag{12}$$

where T_{ref} and p_{ref} are the reference values of the standard state and a_1 and a_2 are fuel-dependent parameters.

The water injected from the water injector forms small droplets and mixes with the gases in the cylinder. The spray model needs to consider the droplet movement, fragmentation, evaporation, and wall impingement. Considering the movement resistance and buoyancy of droplets in the gases, the following equation for the droplet velocity is obtained.

$$\frac{du_{id}}{dt} = \frac{3}{4} C_D \frac{\rho_g}{\rho_d}\frac{1}{D_d}\left|u_g - u_d\right|\left(u_{ig} - u_{id}\right) + \left(1 - \frac{\rho_g}{\rho_d}\right)g_i, \tag{13}$$

where u_{id} is the particle velocity vector, u_{ig} is the domain fluid velocity, C_D is the drag coefficient, D_d is the particle diameter, ρ_g and ρ_d are the densities of the gas and the droplet, and g_i is the gravitational acceleration vector.

The instantaneous droplet position vector can be determined by

$$\frac{dx_{id}}{dt} = u_{id}. \tag{14}$$

The evaporation process of the droplet is described by

$$m_d c_{p,d}\frac{dT_d}{dt} = \dot{Q}\left(1 + L\frac{\dot{f}_{vs}}{\dot{q}_s}\right). \tag{15}$$

Assuming the Lewis number is unity, the flux ratio can be written as

$$\frac{\dot{f}_{vs}}{\dot{q}_s} = \frac{-B_y}{h_\infty - h_s - \left(h_{vs} - h_{gs}\right)\left(Y_{v\infty} - Y_{vs}\right)}, \tag{16}$$

where

$$B_y = \frac{Y_{vs} - Y_{v\infty}}{1 - Y_{vs}}. \tag{17}$$

The convective heat flux supplied from the gas to the droplet is denoted by

$$\dot{Q} = D_d \pi \lambda Nu (T_\infty - T_s). \tag{18}$$

The KH-RT model is used for the breakup process of the droplets. The wavelength Λ and wave growth rate Ω of the fastest growing wave are

$$\Lambda = 9.02r \frac{\left(1 + 0.45Oh^{0.5}\right)\left(1 + 0.4T^{0.7}\right)}{\left(1 + 0.87We_g^{1.67}\right)^{0.6}}. \tag{19}$$

$$\Omega = \left(\frac{\rho_d r^3}{\sigma}\right)^{-0.5} \frac{0.34 + 0.38We_g^{1.5}}{(1 + Oh)\left(1 + 1.4T^{0.6}\right)}. \tag{20}$$

Then, the breakup time is calculated as

$$\tau_a = \frac{3.726C_2 r}{\Lambda\Omega}. \tag{21}$$

Rayleigh-Taylor disturbances are in continuous competition with Kelvin-Helmholtz surface waves. The RT mechanism is caused by quick deceleration of the droplets, resulting in a growth of surface waves. When the droplet diameter is larger than the wavelength of the critical disturbance wave, the process of droplet breakage caused by RT must be considered. The fastest growing frequency Ω_t and wave number K_t are

$$\Omega_t = \sqrt{\frac{2}{3\sqrt{3\sigma}} \frac{g_t |\rho_d - \rho_c|^{1.5}}{\rho_d + \rho_c}}, \tag{22}$$

$$K_t = \sqrt{\frac{g_t |\rho_d - \rho_c|}{3\sigma}}. \tag{23}$$

The corresponding wave length and breakup time are

$$\Lambda_t = C_4 \frac{\pi}{K_t}, \tag{24}$$

$$\tau_t = C_5 \frac{1}{\Omega_t}. \tag{25}$$

The ATKIM model is used for the ignition process in the cylinder, which considers the charge stratification, the available electrical energy, the heat losses to the spark plug, and the influences of turbulence on the early flame kernel.

The AnB model is used for the prediction of autoignition of the air-fuel mixture. The autoignition delay time of the combustible air-fuel mixture can be calculated as

$$\tau_d = A \left(\frac{ON}{100}\right)^{3.4017} p^{-n} e^{\frac{B}{T}}, \tag{26}$$

where ON is the octane number of kerosene and the parameters A, n, and B are calibrated by the measured data of the in-cylinder pressure.

3. Numerical simulation

The numerical model for the combustion process of Rotax 914 engine fuelled with kerosene is established in AVL Fire software based on the mathematical model. The combustion chamber is shown in **Figure 1(a)**. The original engine uses gasoline fuel, and a carburetor-type fuel supply system is installed. In order to ensure a reliable ignition, the combustion chamber employs a double spark plug arrangement. One inlet valve and one exhaust valve are used. Because kerosene is difficult to be evaporated, the fuel injection system is replaced by a port fuel injection (PFI) system in this study. The main technical parameters of the retrofitted engine are listed in **Table 1**. The 3D grid model of the combustion chamber is shown in **Figure 1(b)**. The function of automatic grid generation is adopted, and the grid size is set between 0.5 mm and 1.5 mm. The total number of grids is 363,785. After checking the quality of the grid, the numerical simulation is performed.

This chapter mainly studies the compression and combustion process in the cylinder. To simplify the calculation process, only the crankshaft angle ranging from −160° CA to 70° CA is simulated where both valves are closed. The piston moves between the top dead center (TDC) and the bottom dead center in the cylinder. The mesh of the volume swept by the piston is divided into five different mesh models according to the rotation angle of the crankshaft. Each mesh number is activated under a specified range of crankshaft angle. The mesh number of each

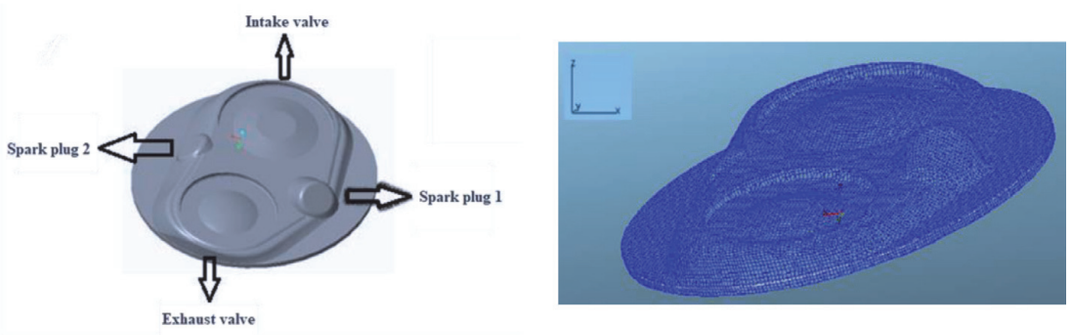

Figure 1.
Combustion chamber of the four-stroke spark-ignition engine: (a) 3D model; (b) volume mesh.

Item	Parameter	Unit
Displacement	1.211	L
Bore × stroke	79.5 × 61	mm
Cylinder number	4	—
Rated power	75	kW
Rated speed	5500	r/min
Max. torque	144	N.m
Speed at max. Torque	4900	r/min
Combustion chamber	Bathtub	
Valve actuation	2 valves per cylinder	
Air-fuel ratio	Stoichiometric	

Table 1.
Specifications of Rotax 914 engine.

mesh model remains unchanged, and only stretching or compression is experienced. The mesh quality in the process of tension or compression is checked. The initial pressure in the cylinder is set as 1.52 bar, and the initial temperature is set to 320 K. The temperatures of the cylinder head, cylinder wall, and piston top surface are set as 400, 380, and 450 K, respectively. The number of orifices for the water injector is six, and the diameter of the orifice is 2 mm.

In order to verify the accuracy of the numerical model, the in-cylinder pressure curve of the original engine with gasoline is simulated and compared with the test results, as shown in **Figure 2**. The engine speed is 5500 r/min and the throttle opening is 30%. The simulated in-cylinder pressure is in good agreement with the experimental one. Only the measured pressure near the TDC is slightly higher than the simulated one. The maximum relative error is 3.58%, which indicates that the numerical model has a high accuracy and can be used for the following simulation of the kerosene combustion process.

For the SI piston engine fuelled with kerosene, the effects of spray time, initial droplet size, and water quantity on knock suppression are analyzed using the established numerical model. The engine speed is set to 5500 r/min and the throttle opening is set to 30%. First, the effect of spray time on detonation suppression is studied. The injected kerosene quantity is fixed at 30 mg. The position of the injector is set in the center of the cylinder. The sprayed water temperature is 300 K and the initial droplet diameter is set to 0.1 mm. Only the starting time of water spray is changed and the other parameters are fixed. The start time of water injection is set as 120°, 80°, and 50° before TDC (BTDC) (represented by T1, T2, and T3, respectively).

The results for the in-cylinder pressure at three different injection times are shown in **Figure 3**. It can be seen that the closer the injection time is to the TDC, the higher the maximum burst pressure in the cylinder is. The useful work of the cycle ascends accordingly. However, the injection time has little effect on the in-cylinder pressure curve as a whole. The maximum pressure difference between T1 and T3 does not exceed 0.5 bar. T3 is close to the TDC and the in-cylinder temperature is higher than T1 and T2. The high temperature in the cylinder makes the liquid water easy to be evaporated. Part of the heat energy of the exhaust gas can be recovered. The combustion speed in the cylinder near the TDC is very fast. The injected water reduces the combustion rate of the combustible mixture. Since the crank angle of T3

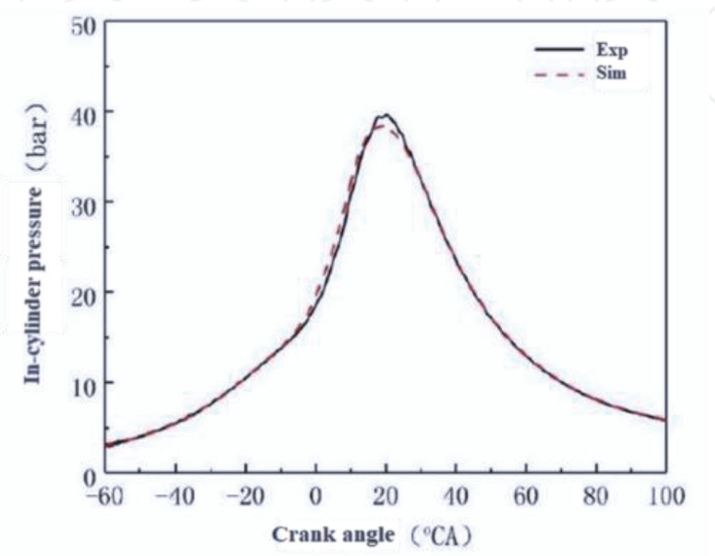

Figure 2.
Comparison of in-cylinder pressure between simulation and experimental data.

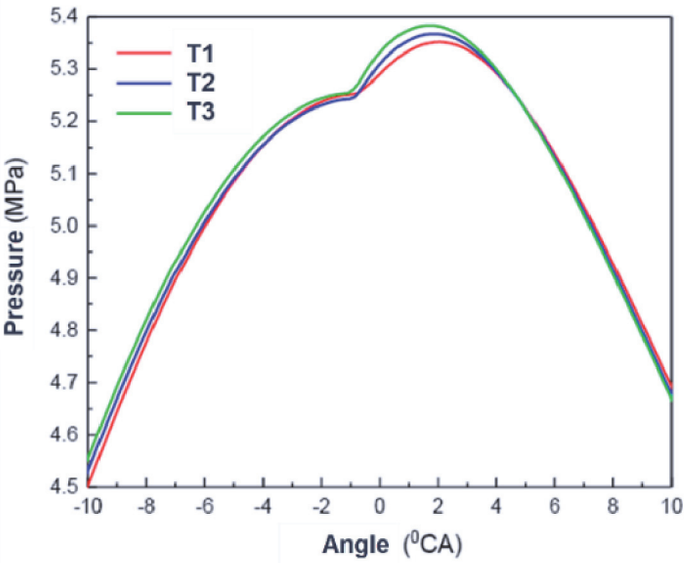

Figure 3.
Results of in-cylinder pressure with different water injection times.

is later than that of T1 and T2, the amount of water vapor in the cylinder is less, and the effect on the reaction rate reduction is the least significant. Therefore, the in-cylinder pressure of T3 is the highest. On the other hand, the closer the injection time is to the TDC, the earlier the phase of peak pressure appears. This is because the injected water vaporizes and absorbs heat in the cylinder and the oxygen concentration in the gas decreases, leading to a decrease of the reaction rate of the combustible mixture. The required compression work also decreases. The farther the injection time is away from the TDC, the longer the duration time of the combustion delay time in the cylinder. Therefore, the peak pressure with water injection time of T1 appears the maximum phase delay. The highest in-cylinder temperature for T1 is about 2300 K, while the highest temperature for T3 reaches 2500 K. The later the start time of water injection, the higher the temperature in the cylinder at the same crankshaft angle (**Figure 4**).

The influence of water injection time on the flame surface density is shown in **Figure 5**. The right spark plug starts to ignite at 52° CA BTDC, and the left spark plug ignites at 40° CA BTDC. The development of the double flames is observed. It can be seen that the flame surface density is greater at the same crank angle if the water injection time is closer to the TDC. The phase for the peak of the secondary heat release rate and the pressure rise rate is advanced accordingly. The peak phase of T3, T2, and T1 is 10°, 8°, and 4° CA BTDC, respectively.

In Fire, an index called combustion knock index (CKI) is used to label the knock intensity inside the cylinder. Generally, an obvious knock happens if the CKI is greater than 20. The results for the CKI under different injection times are shown in **Figure 6**. The CKI values for all the three injection times are maximized and exceed 20 at TDC. The CKI is the smallest for T1 and the strongest for T3. Meanwhile, the phase that the knock starts moves forward if the injection time is late. It can be seen that the knock happens at the position near the cylinder wall far away from the two spark plugs. The detonation phenomenon is reduced after the water injection. With the water injection time advanced from the TDC, the area where the detonation occurs tends to shrink, and the detonation intensity is weakened. This is due to the rapid vaporization of the water droplets after being sprayed into the cylinder, which absorbs a lot of heat in the cylinder. As a result, the in-cylinder temperature decreases. The effects of the compression and radiation of the burnt gas to the end gas reduce accordingly. Therefore, the autoignition time becomes longer than the

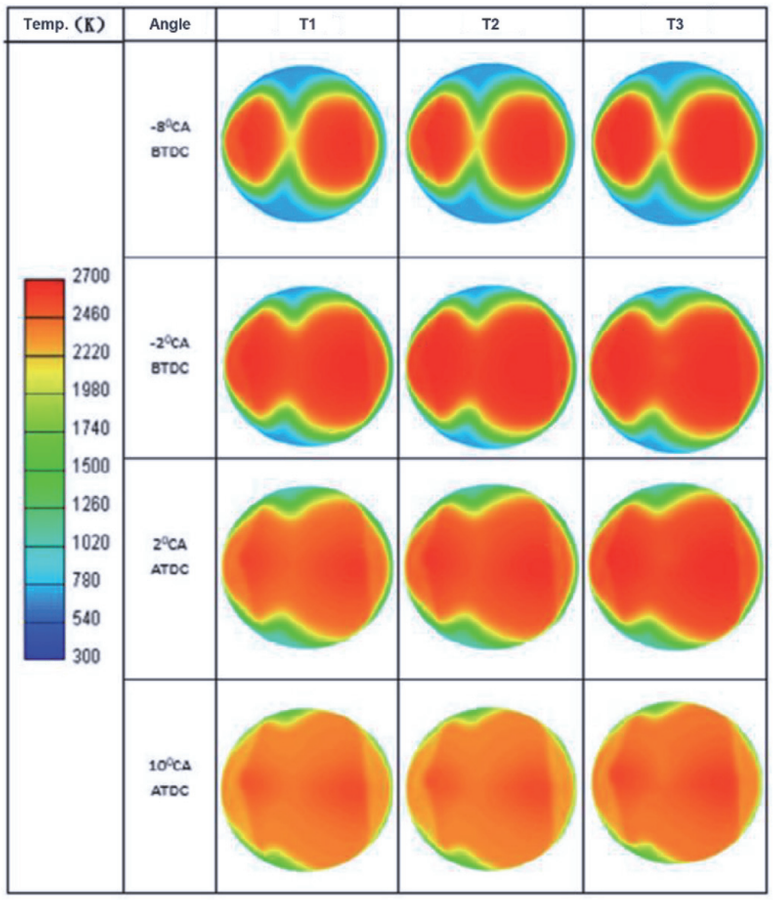

Figure 4.
Results of in-cylinder temperature with different water injection times.

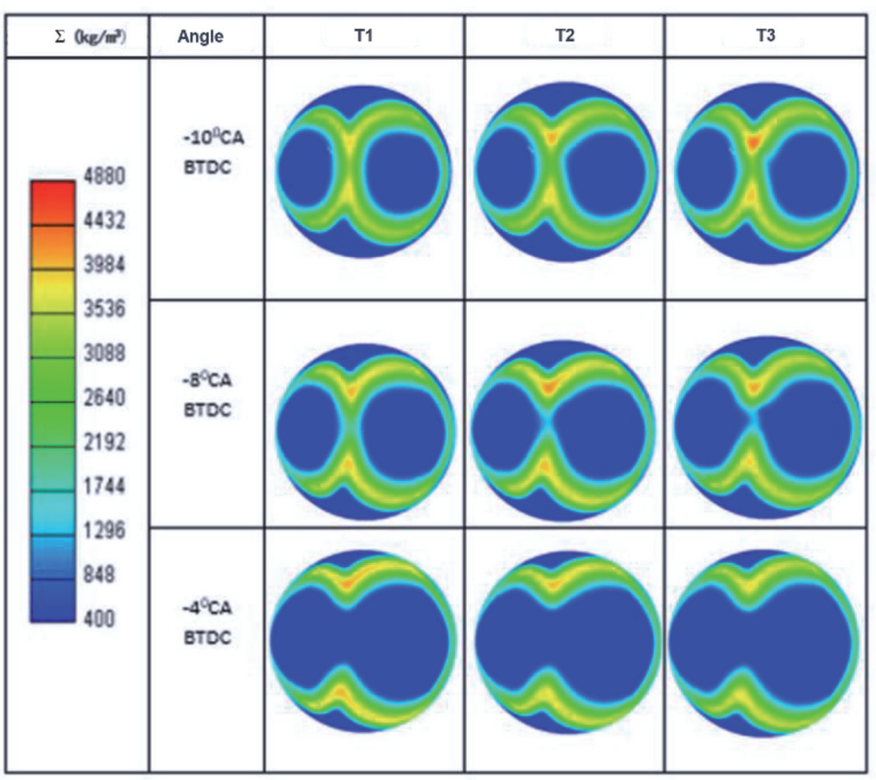

Figure 5.
Results of flame surface density with different water injection times.

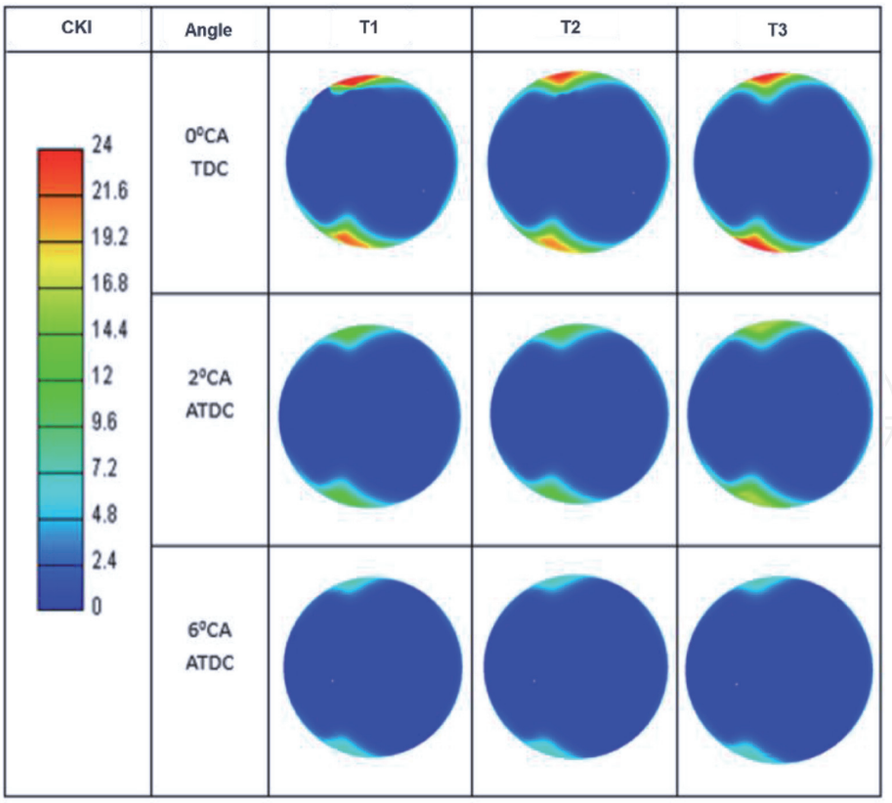

Figure 6.
Results for CKI with different water injection times.

flame propagation time, and the intensity of the detonation drops. Meanwhile, the thermal efficiency reduction caused by the heat loss of the knock phenomenon alleviates. For the aviation kerosene with an octane number of only 40–50, water injection can make the SI engine operate normally without power loss due to the reduced possibility of detonation. Meanwhile, the water injection time must be far enough away from TDC to suppress the knock effectively.

The initial droplet diameter of water spray will affect the subsequent droplet fragmentation and evaporation process. Therefore, it is necessary to study the effect of initial droplet diameter. Based on the above results, the water injection time is set to 120° CA BTDC. The water spray amount is set at 20 mg and the water temperature is set at 300 K. The initial diameters of the water droplets are set to 0.2, 0.1, 0.05, and 0.01 mm, respectively.

Figure 7 shows the influence of the initial droplet diameter on the in-cylinder pressure. The in-cylinder pressure becomes lower if the initial particle size is smaller. When the initial particle size is 0.01 mm, the in-cylinder pressure drops significantly. The in-cylinder peak pressure is about 5.5 MPa for an initial droplet diameter of 0.2 mm. However, when the initial particle size is 0.01 mm, the in-cylinder pressure has been reduced to 4.3 MPa, 21.8% lower than that with an initial droplet diameter of 0.2 mm. This is because the required energy acting on the water droplets to make them deformed and broken is weak for a small droplet diameter if the Weber number and the surface tension coefficient of the water droplet are fixed. When the initial diameter is too large, the energy is not enough to break the droplet, and only the deformation of the droplet occurs. Therefore, only a small part of the droplets with initial droplet diameters of 0.2 and 0.1 mm are broken. Accordingly, the amounts of water vapor are small. Therefore, their influence on the in-cylinder pressure is very limited.

For droplets with an initial diameter of 0.05 mm, there are many modes of fragmentation in the process of atomization. This effectively increases the contact

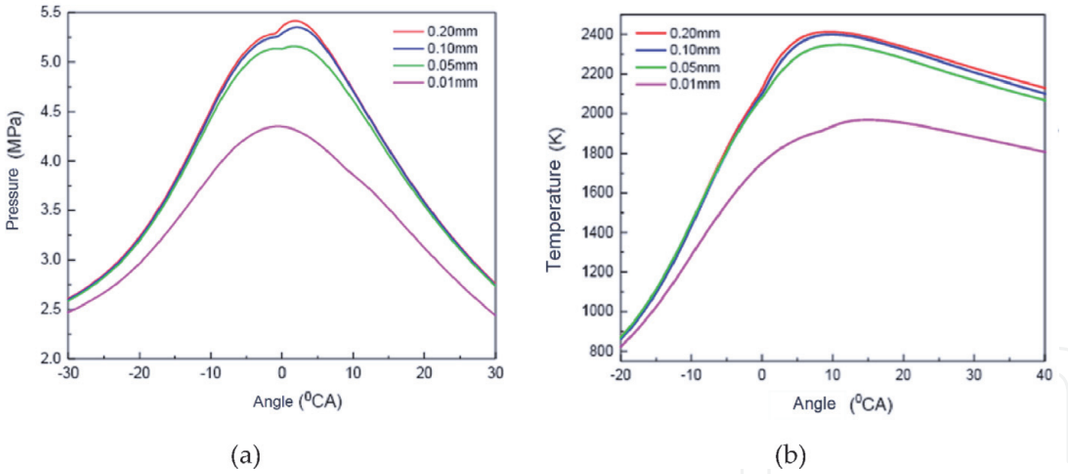

Figure 7.
Results of the in-cylinder pressure (a) and temperature (b) with different initial water droplet diameters.

area between gas and liquid and accelerates the heat transfer rate. When the initial particle size decreases to 0.01 mm, the smaller droplet diameter makes the boundary conditions required for the fragmentation of the droplet smaller, and the critical Weber number becomes smaller. The required energy for the fragmentation and deformation of the droplets is lower. Therefore, the droplet is easier to be broken at this time. The increase of the surface area makes almost all the droplets evaporated, absorbing a lot of heat in the cylinder and reducing the heat release rate and the peak pressure of the combustion process.

The results for the in-cylinder temperature are shown in **Figure 7(b)**. When the initial droplet diameter is between 0.05 and 0.2 mm, the in-cylinder temperature changes slightly with a maximum temperature decrease up to 100 K. However, when the initial particle size is reduced to 0.01 mm, the in-cylinder temperature decreases greatly, and the maximum temperature reduction reaches nearly 500 K.

The results of the cloud chart for knock intensity with different initial droplet diameters are shown in **Figure 8**. The crank angle corresponding to the maximum knock intensity is different. The larger the initial droplet diameter is, the earlier the maximum detonation time will appear. The detonation intensity of the four particle sizes is also different. The larger the initial particle size is, the greater the CKI value of detonation is, indicating that the detonation is more dramatic. The knock phenomenon at the TDC with an initial particle size of 0.2 mm is the most severe, whose CKI value is as high as 30. When the initial droplet diameter is 0.1 mm, the detonation intensity maximizes at 1° CA ATDC, and the occurrence area is smaller. When the initial diameter is 0.05 mm, the maximum detonation happens at 2° CA ATDC, and the occurrence area is reduced apparently. The CKI value is decreased to around 20. When the initial droplet diameter is 0.01 mm, the detonation takes place at 10° CA ATDC. The corresponding CKI value drops to 12, which is reduced by 60% compared with an initial particle size of 0.2 mm.

The main purpose of spraying water into the cylinder is to reduce the temperature in the cylinder to suppress the knock. The amount of water injection directly affects the temperature reduction in the cylinder. Finally, the influence of water injection quantity is analyzed.

Figure 9(a) shows the results of the in-cylinder pressure under different water injection quantities. The in-cylinder pressure generally decreases with the increase of water spray quantity. The maximum burst pressure is 5.4 MPa when no water is sprayed. When the water injection quantity is 20 mg, the maximum burst pressure is 5.1 MPa, which is 5% lower than that without water injection. Furthermore, the

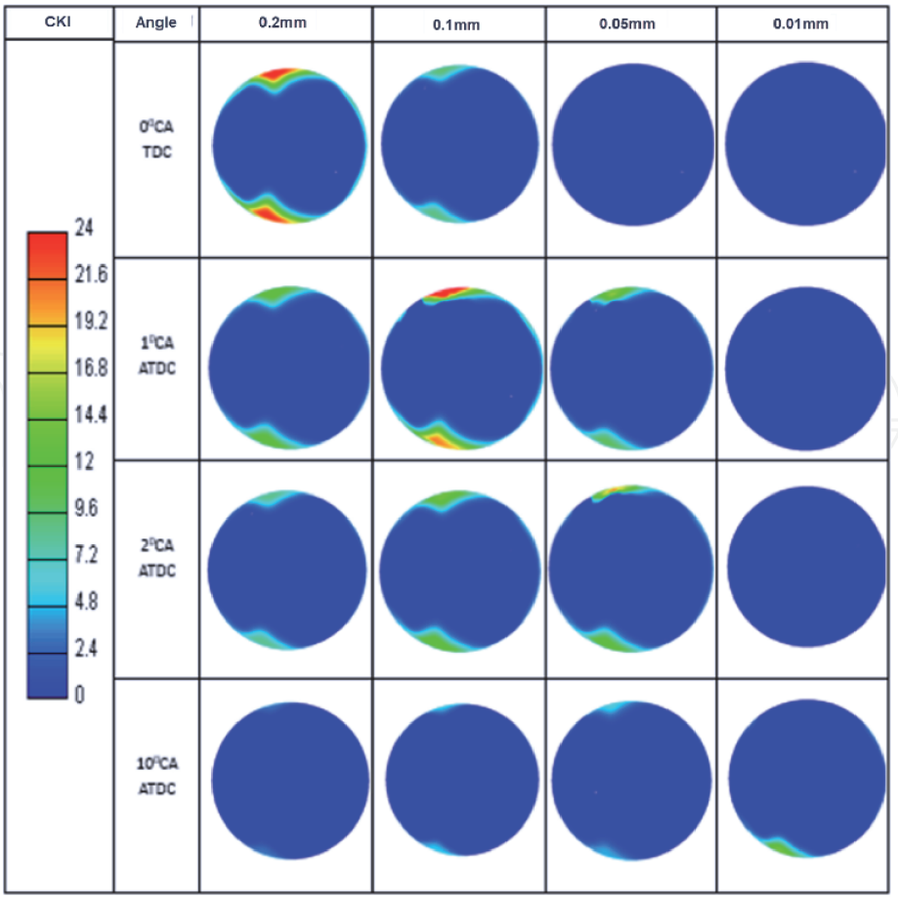

Figure 8.
Results of CKI with different initial water droplet diameters.

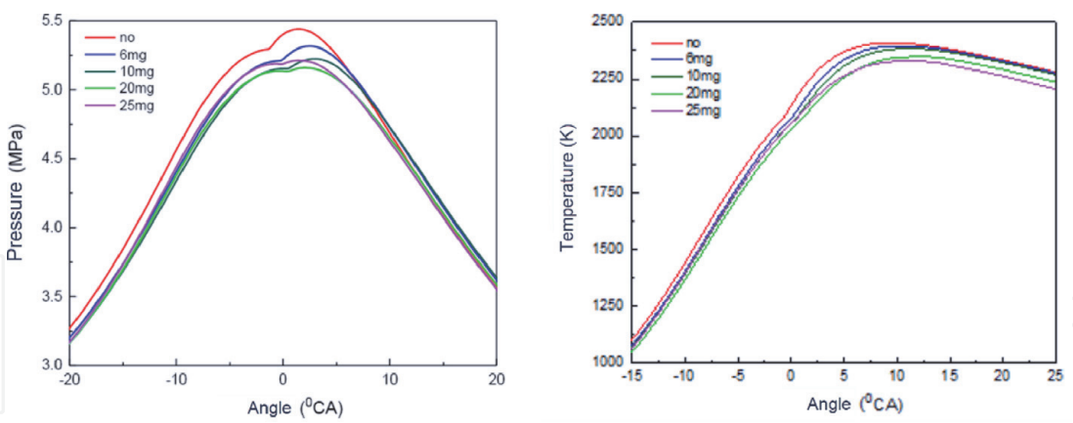

Figure 9.
Results of the in-cylinder pressure (a) and temperature (b) with different amounts of water injection.

larger the amount of water injection is, the later the phase of the maximum burst pressure appears.

Figure 9(b) gives a comparison of the in-cylinder temperature. When there is no water spray, the maximum average temperature in the cylinder is 2408 K. The temperature reduction in the cylinder is increased as the amount of water injection rises. When the water spray is 10 mg, the maximum temperature in the cylinder is 2365 K, which is 43 K lower than that without water spray. When the amount of the water spray is 25 mg, the maximum in-cylinder temperature drops to 2297 K, which is 111 K lower than that without water spray. In the case of water injection, the rise

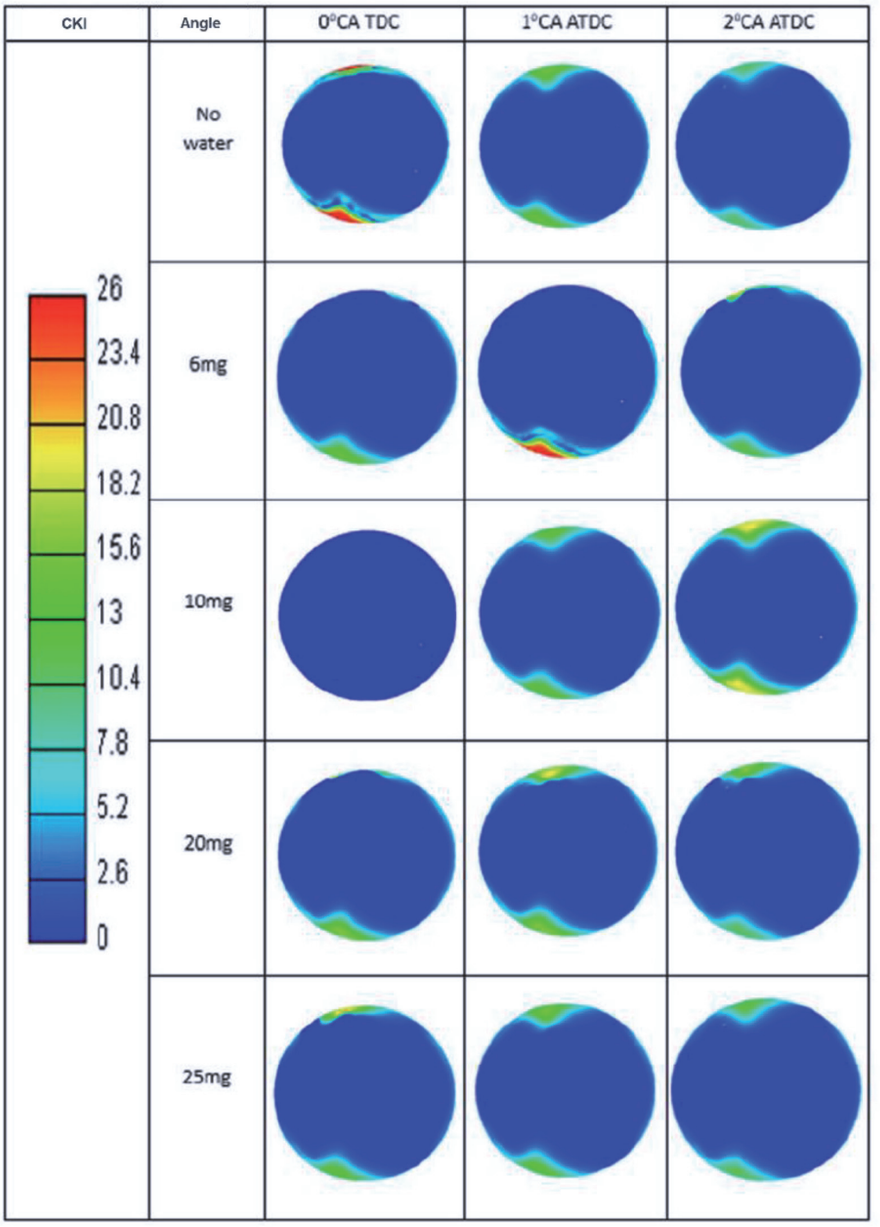

Figure 10.
Results of CKI with different initial water droplet diameters.

rate of the in-cylinder temperature slows down obviously. This is because after injection, water absorbs the heat in the cylinder and reduces the temperature.

The results for the cloud charts of CKI value with different water amounts are shown in **Figure 10**. The maximum CKI value decreases with the increase of water spray. The CKI value without water injection is as high as 26. When the water injection amount is 20 mg, the CKI value is reduced to 18, which is 31% lower than that without water injection.

4. Experimental results

To explore the effect of water injection on knock suppression of SI engine fuelled with kerosene, an engine experiment is carried out [23]. First, the original Rotax 914 engine was modified, and the engine test rig was built, as shown in **Figure 11**. The fuel supply system is first transformed into a PFI kerosene supply

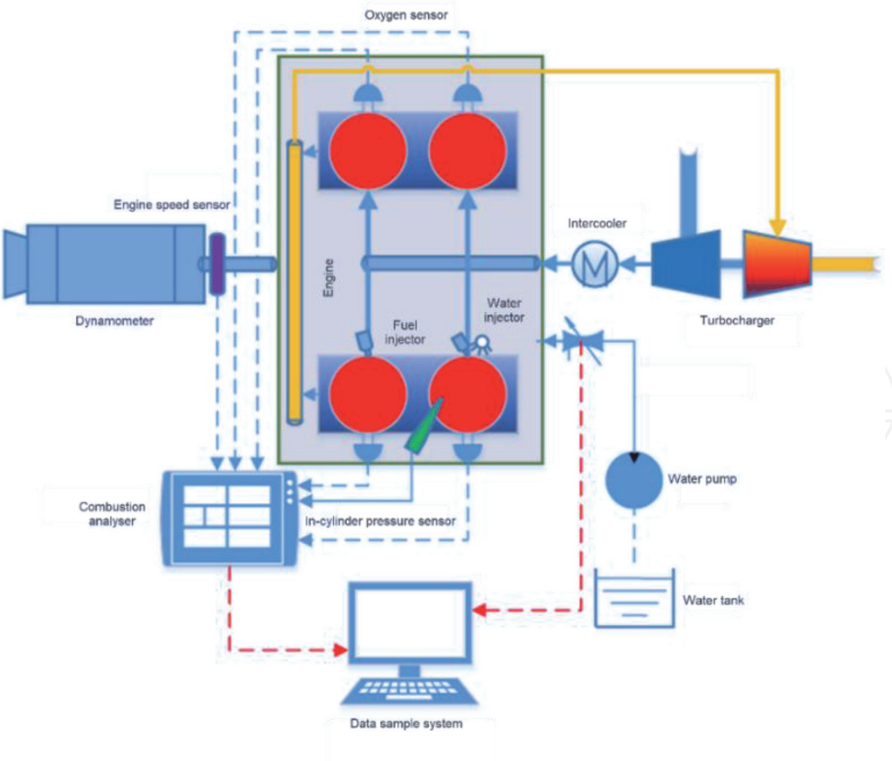

Figure 11.
Schematic of the engine test bench for the SI engine fuelled with kerosene together with water injection.

system. Meanwhile, a water injection system is added, which includes a water injector, a water pump, a water tank, and related pipelines. The water injector is installed at the intake manifold. Since the flame propagation speed of kerosene is significantly lower than that of gasoline, the ignition system of the original engine is modified. One of the spark plugs is replaced with a jet ignition device, as shown in **Figure 12**. The jet combustion pre-chamber uses the small orifices on the surface to inject the jet flame into the main combustion chamber and forms strong turbulent flames. As a result, the flame propagation distance is shortened, and the combustion speed is effectively accelerated. The volume of the jet ignition pre-chamber is 1.5 ml, and the diameter of the six holes on the surface is 1.5 mm.

The output power of the engine is absorbed by an eddy current dynamometer. During the test, kerosene is supplied to the first and third cylinders of the engine, and the original gasoline supply system is used for the second and fourth cylinders. A pressure sensor is installed in the first cylinder to measure the in-cylinder

Figure 12.
Photo of the jet ignition pre-chamber.

pressure. An engine speed sensor is installed at the crankshaft end. The collected data are sent to the combustion analyzer to calculate the heat release rate of the combustion process. **Table 2** lists the main equipment and relative accuracy of the test system.

When the engine speed is 5500 r/min and the throttle opening is 30%, the duration of water injection is set to 0, 2, and 4 ms, respectively. The results of the in-cylinder pressure are shown in **Figure 13(a)**. In the case of no water spray, the maximum pressure in the cylinder reaches 33.9 bar and fluctuates apparently near the TDC with an amplitude of 7.53 bar, indicating that the unburnt end gas in the cylinder is self-ignited and the knock phenomenon occurs. With water injection of 2 ms, the knock phenomenon has been alleviated, and the maximum in-cylinder pressure is increased from 33.9 to 35.4 bar. When the duration of water injection is increased from 2 to 4 ms, the pressure fluctuation in the cylinder caused by kerosene detonation disappears completely, while the maximum burst pressure in the cylinder decreases to 32.5 bar. The corresponding IMEP values are shown in **Figure 13(b)**, which also indicates that the in-cylinder pressure decreases significantly with the increase of water injection quantity.

Subsequently, the limit of knock suppression by water injection is studied under three different engine speeds of 4500, 5000, and 5500 r/min. For each engine speed, the throttle opening and the kerosene injection quantity as well as water injection quantity are increased continuously. The data are recorded until the maximum water injection duration is arrived. **Figure 14(a)** shows the comparison of kerosene injection quantity. In the case of no water injection, the maximum kerosene injection quantity under the three different engine speeds is about 20 mg. If the injection quantity exceeds this value, there will be an obvious detonation. The

Equipment	Model	Accuracy
Eddy current dynamometer	China Kaimai CW 160	<±0.5%
Fuel meter	Japan Ono MF-2200	<1%
Cylinder pressure sensor	Kistler 6115	<±0.5%
Lambda sensor	Bosch LSU4.9	<1%
Combustion analyzer	Kibox 2893	<1%

Table 2.
Main facilities of the experimental system.

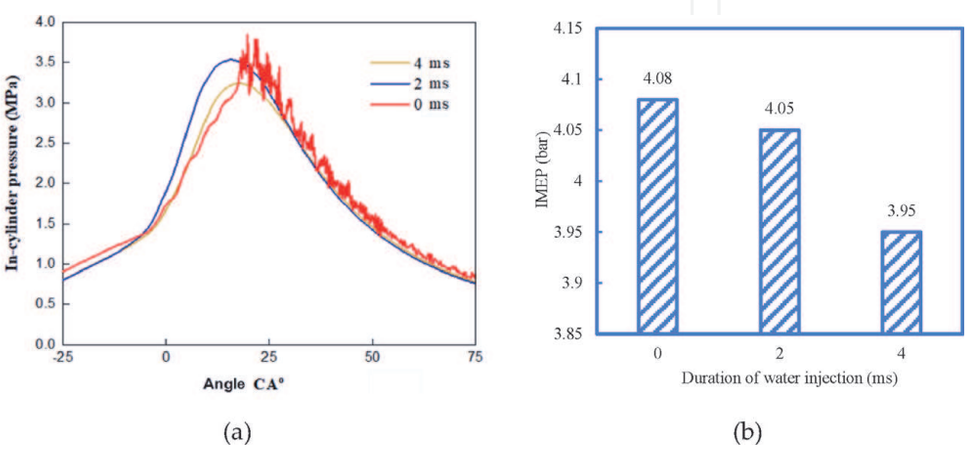

Figure 13.
Results for the in-cylinder pressure (a) and IMEP (b) with different water injection durations.

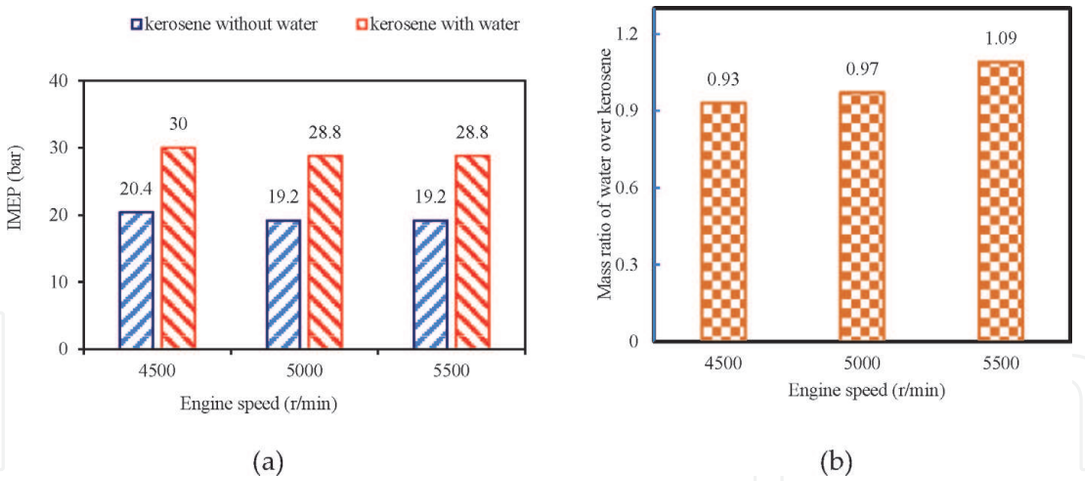

Figure 14.
Results for the maximum amount of injected kerosene with/without water injection under different engine speeds (a) and the mass ratio of water over kerosene (b).

maximum kerosene injection quantity is increased by about 50% with water injection. The corresponding mass ratios of the sprayed water over kerosene are shown in **Figure 14(b)**. It can be seen that the mass ratio is close to 1:1 at three engine speeds.

Figure 15 shows the comparison of IMEP improvement under three different engine speeds. The IMEP can be increased from less than 8 to nearly 10 with water injection for each engine speed. The results show that using water injection can improve the kerosene injection quantity, leading to an increase of the IMEP and the power output of the engine. This is because after spraying water, the liquid water evaporates and absorbs heat, and the temperature in the cylinder decreases. Accordingly, the compression and radiation effect of the burnt gas imposed on the unburnt end gas weakens, and the autoignition time becomes longer, avoiding the violent detonation. The allowable charge of fresh mixture in the cylinder increases. Thus, more fuel can be injected and the engine's output power is improved. Meanwhile, it can be seen that the IMEP of the original engine with gasoline can reach 13 bar, and the IMEP of the kerosene fuel with water spray still needs to be enhanced.

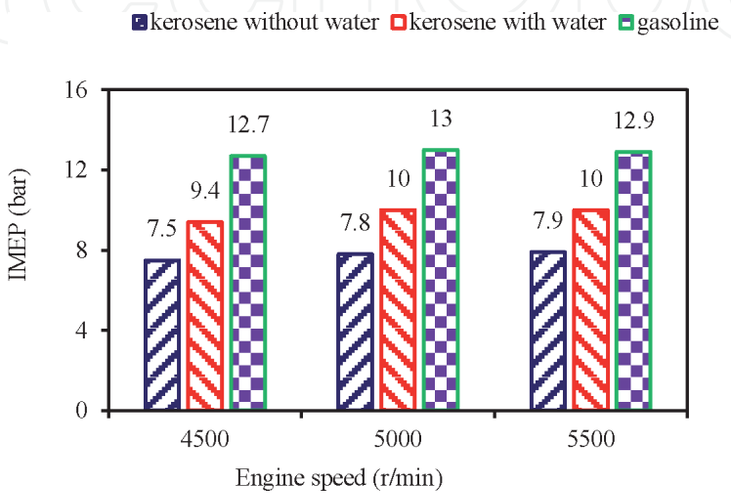

Figure 15.
Maximum improvements of the IMEP for the engine fuelled with kerosene together with water injection.

5. Conclusions

In this chapter, the feasibility of knock suppression using water injection for an SI engine fuelled with kerosene is investigated. First, a 3D numerical model is established in AVL Fire software. The influences of water injection timing, initial droplet diameter, and water injection quantity are analyzed. Then, an engine experiment is performed to evaluate the limit of IMEP improvement.

The results indicate that water injection can suppress the knock of kerosene effectively. The water injection timing should be advanced and far away from TDC because the evaporation of water droplets needs time. Accordingly, a lower pressure rise rate can be obtained, and the phase angle of the peak pressure can be postponed. The autoignition time enlarges, the flame propagation speed drops, and the intensity of the detonation decreases, due to a reduction of in-cylinder temperature. Meanwhile, a better result of knock suppression can be obtained with a smaller initial water droplet diameter, owing to a larger evaporation surface area of droplets. With the increase of the water injection amount, the reduction of in-cylinder temperature increases. The allowable throttle opening and injected kerosene amount also increase, resulting in a significant increase of the IMEP. The experimental results show that the maximum IMEP is improved from about 8 to 10 bar with an engine speed of 5500 r/min. However, an excessive water injection will lead to a decrease of the IMEP. To evaluate the effect of water injection comprehensively, an optimization design of the water injection system and the combustion chamber geometry is required. Meanwhile, more experimental work should be carried out, especially for the practical operation conditions of an unmanned aerial vehicle.

Acknowledgements

The authors would like to thank for the support of the National Natural Science Foundation of China (Grant No. 51876009).

Conflict of interest

The authors declare no conflict of interest.

Acronyms

3D	three-dimensional
SI	spark ignition
ATDC	after top dead center
BTDC	before top dead center
CKI	combustion knock index
GDI	gasoline direct injection
IMEP	indicative mean effective pressure
LIF	laser-induced fluorescence
ON	octane number
PFI	port fuel injection
PM	particle material
NOx	nitrogen oxide
TDC	top dead center

IntechOpen

IntechOpen

Author details

Enhua Wang*, Chenyao Wang, Fujun Zhang, Huasheng Cui, Chuncun Yu, Bolan Liu, Zhenfeng Zhao and Changlu Zhao
School of Mechanical Engineering, Beijing Institute of Technology, Beijing, China

*Address all correspondence to: enhua.wang@yahoo.com

IntechOpen

© 2020 The Author(s). Licensee IntechOpen. This chapter is distributed under the terms of the Creative Commons Attribution License (http://creativecommons.org/licenses/by/3.0), which permits unrestricted use, distribution, and reproduction in any medium, provided the original work is properly cited. CC BY

References

[1] Rozenkranc M, Ernst J. Tactical UAV engines integration in IAI. In: 2nd AIAA "Unmanned Unlimited" Systems, Technologies, and Operations — Aerospace; 15-18 September 2003, San Diego, California

[2] Yu W, Yang W, Zhao F. Investigation of internal nozzle flow, spray and combustion characteristics fueled with diesel, gasoline and wide distillation fuel (WDF) based on a piezoelectric injector and a direct injection compression ignition engine. Applied Thermal Engineering. 2017;**114**: 905-920

[3] Zeng W, Li H, Chen B, Ma H. Experimental and kinetic modeling study of ignition characteristics of Chinese RP-3 kerosene. Combustion Science and Technology. 2015;**187**: 396-409

[4] Cooke JA, Bellucci M, Smooke MD, Gomez A, Violi A, Faravelli T, et al. Computational and experimental study of JP-8, a surrogate, and its components in counterflow diffusion flames. Proceedings of the Combustion Institute. 2005;**30**:439-446

[5] Shao J, Zhu Y, Wang S, Davidson DF, Hanson RK. A shock tube study of jet fuel pyrolysis and ignition at elevated pressures and temperatures. Fuel. 2018; **226**:338-344

[6] Burkert A, Paa W. Ignition delay times of single kerosene droplets based on formaldehyde LIF detection. Fuel. 2016;**167**:271-279

[7] Felden A, Esclapez L, Riber E, Cuenot B, Wang H. Including real fuel chemistry in LES of turbulent spray combustion. Combustion and Flame. 2018;**193**:397-416

[8] Fan X, Yu G, Li J, Zhang X. Investigation of vaporized kerosene injection and combustion in a supersonic model combustor. Journal of Propulsion and Power. 2006;**22**:103-110

[9] Teoh YH, Masjuki HH, Kalam MA, Amalina MA, How HG. Impact of premixed kerosene fuel on performance, emission and combustion characteristics in partial HCCI engine. Energy Procedia. 2014;**61**:1830-1834

[10] Tay KL, Yang W, Zhao F, Yu W, Mohan B. A numerical study on the effects of boot injection rate-shapes on the combustion and emissions of a kerosene-diesel fueled direct injection compression ignition engine. Fuel. 2017; **203**:430-444

[11] Tay KL, Yang W, Li J, Zhou D, Yu W, Zhao F, et al. Numerical investigation on the combustion and emissions of a kerosene-diesel fueled compression ignition engine assisted by ammonia fumigation. Applied Energy. 2017;**204**:1476-1488

[12] Fernandes G, Fuschetto J, Filipi Z, Assanis D, McKee H. Impact of military JP-8 fuel on heavy-duty diesel engine performance and emissions. Proceedings of the Institution of Mechanical Engineers, Part D. 2007; **221**(8):957-970

[13] Tay KL, Yang W, Mohan B, An H, Zhou D, Yu W. Development of a robust and compact kerosene–diesel reaction mechanism for diesel engines. Energy Conversion and Management. 2016;**108**: 446-458

[14] Wang Z, Liu H, Reitz RD. Knocking combustion in spark-ignition engines. Progress in Energy and Combustion Science. 2017;**61**:78-112

[15] Hoppe F, Thewes M, Baumgarten H, Dohmen J. Water injection for gasoline engines: Potentials, challenges, and

solutions. International Journal of Engine Research. 2016;**17**(1):86-96

[16] Battistoni M, Grimaldi CN, Cruccolini V, Discepoli G. Assessment of port water injection strategies to control knock in a GDI engine through multi-cycle CFD simulations. SAE Technical Paper 2017-24-0034

[17] Miganakallu N, Naber JD, Rao S, Atkinson W, Barros S. Experimental investigation of water injection technique in gasoline direct injection engine. In: Proceedings of the ASME 2017 Internal Combustion Engine Division Fall Technical Conference; October 15-18 2017. Seattle, Washington, USA

[18] Kim J, Park H, Bae C, Choi M, Kwak Y. Effects of water direct injection on the torque enhancement and fuel consumption reduction of a gasoline engine under high-load conditions. International Journal of Engine Research. 2016;**17**(7):795-808

[19] Wei M, Sa NT, Turkson RF, Liu J, Guo G. Water injection for higher engine performance and lower emissions. Journal of the Energy Institute. 2017;**90**(2):285-299

[20] Anderson EK, Brown AC, Baranski J, Hoke JL. Performance of low-octane fuels in a Rotax 914 engine with advanced knock mitigation strategies. In: 47th AIAA/ASME/SAE/ASEE Joint Propulsion Conference & Exhibit; 31 July–3 August 2011. San Diego, California

[21] Baranski J, Anderson E, Grinstead K, Hoke J, Litke P. Control of fuel octane for knock mitigation on a dual-fuel spark-ignition engine. SAE Technical Paper 2013-01-0320

[22] Anderson EK, Attard WP, Brown A, Litke P, Grinstead K, Hoke J. Experimental study of a pre-chamber jet igniter in a turbocharged Rotax 914 aircraft engine. SAE Technical Paper 2013-01-1629

[23] Wang C, Zhang F, Wang E, Yu C, Gao H, Liu B, et al. Experimental study on knock suppression of spark-ignition engine fuelled with kerosene via water injection. Applied Energy. 2019;**242**: 248-259